Electrical coupling analysis of 2D time-multiplexing memory actuators exhibiting asymmetric butterfly hysteresis

Schmerbauch, Anja E. M.; Vakis, Antonis I.; Jayawardhana, Bayu

Published in:
Journal of Applied Physics

DOI:
10.1063/5.0062981

Publication date:
2021

Electrical coupling analysis of 2D time-multiplexing memory actuators exhibiting asymmetric butterfly hysteresis

A. E. M. Schmerbauch,[a] A. I. Vakis, and B. Jayawardhana
Engineering and Technology Institute Groningen, Faculty of Science and Engineering, University of Groningen, 9747AG Groningen, The Netherlands

We present the modeling and analysis of electrical coupling in a hysteretic deformable mirror with 2D memory piezoactuators, which are made of a purposely-designed piezomaterial sandwiched between electrodes arranged crosswise and actuated by a multiplexing approach. Using a modified Miller model to describe the memory effect which is based on the ferroelectric domain switching processes, the proposed framework is used to simulate the electric field dependence of the strain in the piezoelectric material that exhibits asymmetric butterfly loops with remnant deformation through the finite element method. The desired butterfly memory effect in the material is obtained by modifying the saturated dipole polarization curve in the Miller model. The proposed method allows us to numerically investigate the electrical coupling between actuators in more detail and correspondingly understand their influence to the mirror facesheet.

I. INTRODUCTION

Deformable mirrors (DMs) have been designed and deployed to control wavefronts precisely in optical systems. Their reflective surface can be shaped by controlling the actuators, placed underneath in an array, through an applied electric field. In space-based astronomical instruments, DMs are critical components in the adaptive optics and are required to meet the extreme wavefront control requirements for high contrast imaging of exoplanets with coronographic instruments. While their performance increases as the density of actuators increases, scaling of the current DM designs to the needed capabilities remains challenging[1,2].

New solutions and technologies are developed for realising high actuator densities in DMs[3,4] as well as novel materials tested and manufactured[5–8]. A recently presented concept of a hysteretic deformable mirror (HDM)[9] for an exoplanet-imaging space mission opens up the possibility of deploying an extremely dense actuator array where 2D memory piezoactuators are realized by placing a newly developed piezoelectric shape memory material between two orthogonal layers of electrodes as illustrated in Figure 1. In this configuration, any pair of top and bottom electrodes constitutes a single piezoactuator that can be actuated by applying a local electric field through this pair of electrodes. Correspondingly, each actuator can be addressed independent to the others through a set-and-forget principle and by time division multiplexing (TDM).

While local electric fields can be applied to actuate any piezoactuator via the corresponding pair of electrodes, the electrode array configuration can introduce undesirable electrical coupling and is a critical aspect in the design and working principle of the HDM. The relationship between surface profile and voltage distribution needs to be studied[10]. Particularly, neighboring actuators can become electrically coupled due to the distribution of the electric potential within the piezoelectric memory material used as a base structure when one single actuator is addressed. If the electric field strength

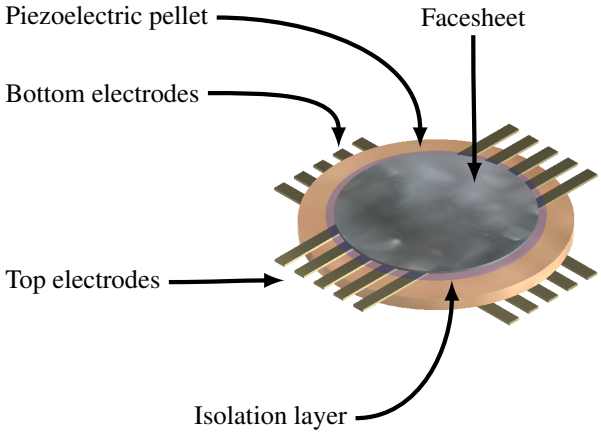

FIG. 1: Conceptual visualization of the hysteretic deformable mirror consisting of a piezoelectric PNZT ceramic pellet as base structure and electrode grids perpendicular to each other forming the actuators at the intersections. On top an isolation layer and the reflective facesheet are placed.

at these neighboring actuators is too high, the remnant deformation will be activated and an additional displacement in crossline grids around the addressed actuator will affect the mirror facesheet and degrade the precision of the HDM. Correspondingly, in order to investigate the limiting effect of the electrical coupling on the HDM concept, we present in this paper: 1) numerical modeling and analysis of an individual piezoactuator of the HDM that incorporates the asymmetric hysteresis property of our piezoelectric shape memory material; and, 2) numerical validation on the behavior of the memory material and electrical coupling between actuators based on an integrated high-fidelity multiphysics model of the HDM simulated via a multiphysics software. In our first contribution, we present a modified Miller model to describe accurately the memory effect of our piezomaterial in a single actuator. The model is used to show the electric-field dependence of the strain in the material that can exhibit the measured asymmetric butterfly loops with remnant deformation. In our second contribution, we integrate the modified Miller model with the piezoelectric material nodes of Comsol

[a]Author to whom correspondence should be addressed. Electronic mail: a.e.m.schmerbauch@rug.nl

Multiphysics that we use to build the integrated model of the HDM. Our integrated multiphysics simulation results confirm that the electrical coupling in the current array configuration can introduce undesirable displacement. It mainly affects the actuators on the crosslines whose positions are set at approximately 25% of the addressed actuator's memory position after direct addressing of the remnant displacement. The simulation results show a lower cross-coupling effect than the initial estimate of 50% that is used in the previous closed-loop control systems simulation in Ref. 9. Another notable observation from additional simulations is that this phenomenon can permeate the whole actuator array when a pair of electrodes undergoes multiple cycles of applied electrical field. Further studies are required on the long-term operations of the HDM.

This paper is organized as follows: Section II presents the theoretical background of the individual component subsystems such as modeling of the mechanical system, hysteresis modeling, and a framework for optimization work within the design based on a sensitivity analysis. In Section III the simulation results of the integrated system in its full complexity are presented, and are discussed in Section III D. Finally, the conclusions are given in Section IV.

II. THEORETICAL FRAMEWORKS

Section II presents the theoretical background on modeling the HDM with its shape memory material and hysteresis, and discusses the electrical coupling of actuators with the aid of different criteria for its influence.

A. Model of the hysteretic deformable mirror

The HDM is characterized by a high actuator density and a compact design which requires only a single high voltage amplifier to address the actuators through TDM. The conceptual visualization of a demonstrator can be found in Figure 1. The base structure of the mirror corresponds to a piezoelectric $PbNb_{0.04}(Ti_{0.48}Zr_{0.52})_{0.96}O_3$ pellet called PNZT[9,11] with thickness t_p. This purposely-designed material is based on lead zirconate titanate and belongs to the group of piezoelectric ceramics[12–17] which is characterized by superior ferroelectric and piezoelectric properties[18,19]. PNZT is a highly nonlinear material that has a strain memory effect, meaning that there are two stable piezoelectric strain states at zero field[20]. Consequently, this material has an asymmetric Strain - Electric field (S-E) loop, which is commonly known as butterfly hysteresis loop. This asymmetry has been achieved by application of niobium as soft dopant[21]. The origin of the remanent strain is the internal electrical field induced by the electrode configurations and the result of the ferroelectric domain state which is not symmetrically switched during its application. An example of such a hysteresis loop and its corresponding polarization loop from experimental data are presented in Figure 2. The memory effect amounts to approximately 40% of the maximum deformation of the material.

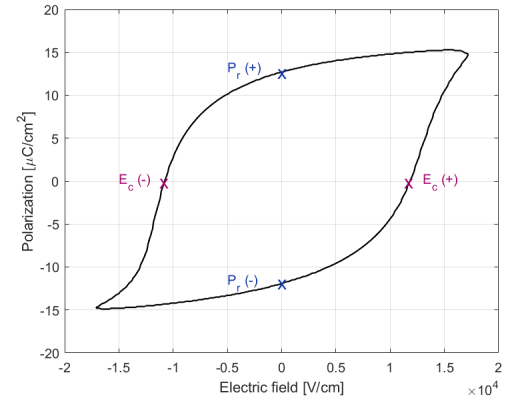

(a) Polarization loop

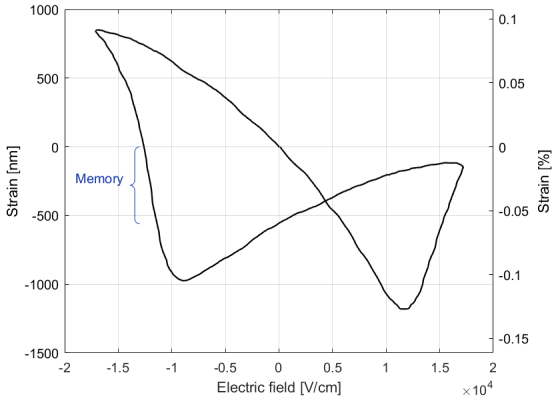

(b) Butterfly loop

FIG. 2: Polarization (a) and hysteresis loop (b) of a common PNZT pellet used for the HDM showing the significant points of the remnant polarization P_r, coercive field E_c and the memory effect.

On the top and bottom there are electrode grids which consist of several strips that are perpendicular to each other and, therefore, define $n \times m$ actuators, where n is the number of bottom electrode strips and m is the number of top electrode strips. This electrode layout offers the possibility to make use of TDM and transmit and receive independent signals over shared electrodes in periodic intervals. Due to this method, only a single amplifier per layer is needed instead of $n+m$ (when we consider each strip to be energised independently) or $n \times m$ (when we consider the use of standard piezoactuators that must be actuated independently). This leads to a compact and lightweight design. On the surface of the upper electrode grid, a thin isolation layer with thickness t_s and a reflective top layer, named the facesheet, with thickness t_f are mounted. The isolation layer is in contact with the upper electrode grid.

To address one actuator, an electric potential is applied to the top electrode while the bottom electrode is grounded. Due to the distribution of the electric field within the piezoelectric pellet, neighboring actuators can become electrically coupled. Previous simulations, which deploy simplified models based on standard PZT materials without memory effect and station-

ary analyses for pellets[22] and thin layers[9], show a surrounding cross-coupling of up to 50%. Since these high values of cross-coupling could present a serious limitation for the presented concept, we investigate the electrical coupling in combination with the memory for elucidating their influences on the performance of the HDM. Therefore, we distinguish between two criteria, namely the primary influence and the secondary influence.

The primary influence reflects the case when the activation threshold for the surrounding actuators of the addressed one is reached and a cross-coupling is evoked so that additional deformations on the facesheet at other actuator positions are visible. This would lead to the inability to shape the mirror according to the desired modes and requires a complicated control architecture to adjust the leveling of electrically coupled actuators and reset them individually to their intended positions.

The secondary influence presents the case where the activation threshold is on the borderline and might lead to small effects in the operating behavior. Here, the problem could be addressed by optimizing the design: changing t_s and t_f to tweak the mechanical coupling between actuators on the facesheet. By calibrating the mechanical coupling to a range from local to global interaction, small cross-coupling deformations at surrounding actuators can be covered. For this, a sensitivity analysis is proposed in Section II C studying the divide and allocation of uncertainty between the maximum deformation of the mirror facesheet to different sources of uncertainty in its layer thickness and the mechanical properties.

If the activation threshold is not reached, an undesired deformation profile is not expected in relation to the memory material and a limiting effect can be excluded.

B. Modeling of the memory material

Hysteresis occurs in ferromagnetic materials, ferroelectric and piezoelectric materials, shape-memory alloys and numerous other natural systems and phenomena. It is characterized by its nonlinearity, and often involves memory. While the piezoelectric strain hysteresis is a nonlinear phenomenon between the applied electric field and the output displacement, the hysteresis in ferroelectrics is mostly caused by the irreversible displacement of domain walls involving many mechanisms that depend on the nature of the ferroelectric material itself. The presence of butterfly loops has been shown and observed e.g. in piezoelectric actuator systems[23] and magnetostrictive materials[24]. A number of models have been proposed in the literature that describe the hysteresis behavior well[25–28].

We study a class of theoretical approaches to model memory materials with remnant deformation and butterfly hysteresis behavior, which are suitable for implementation in finite element analysis and multiphysics simulation software. Common ferroelectric materials have two states of polarization and can switch between them when an external field is applied. For example, an applied positive voltage V leads to a positive state of polarization p^+ and an applied negative voltage $-V$ to a negative state of polarization p^- due to the switching of dipole orientation. While in ferroelectricity the source of polarization is the dipole interaction energy itself, in piezoelectricity the crystal is polarized by the application of an external stress.

Considering a ferroelectric capacitor, the increase of the positive polarization state can be given by the following equation[29]

$$\Delta p^+ = (1-p^+) f^+ \Delta V \tag{1}$$

where Δp is the incremental change of the state, ΔV the incremental voltage and $f^+\Delta V$ the transition probability for the case when the amount of negative polarization becomes a positive tendency when a positive voltage is applied. Moreover,

$$f^+ = \frac{1}{1+e^{\frac{-(V-V_c)}{V_0}}} \frac{1}{V_0} \tag{2}$$

where V_c and V_0 are the coercive voltage and thermal voltage, respectively. Based on Eq. (1) and Eq. (2), the analytical expression for the positive and negative polarization state is obtained[29]

$$\begin{aligned} p^+ &= 1-(1-p_i^+)\frac{1+e^{\frac{(V_i-V_c)}{V_0}}}{1+e^{\frac{(V-V_c)}{V_0}}} \\ p^- &= 1-(1-p_i^-)\frac{1+e^{\frac{(V_i-V_c)}{V_0}}}{1+e^{\frac{(-V-V_c)}{V_0}}} \end{aligned} \tag{3}$$

where V_i is the initial voltage and $p_i^{+/-}$ is the initial increasing/ decreasing polarization state. Hence, the electric displacement D for positive and negative applied voltages can be given by

$$\begin{aligned} D^+ &= P_{\text{sat}}(2p^+ - 1) \\ D^- &= -P_{\text{sat}}(2p^- - 1) \end{aligned} \tag{4}$$

where P_{sat} denotes the saturation polarization.

Miller[30,31] presented a differential hysteresis model which can simulate the polarization-field (D-E) response to deal with arbitrary applied fields, in which minor unsaturated loops are modeled by scaling the major saturated loop. The model has three parameters which are the coercive field E_c, remanent polarization P_r and spontaneous polarization P_s, and does not consider history-dependent effects. Based on this model of a ferroelectric capacitor with saturated dipole polarization hysteresis loop[30], the derivative of the dipole polarization is given by

$$\frac{\partial P_d}{\partial E} = \Gamma \frac{\partial P_{\text{sat}}}{\partial E} \tag{5}$$

where P_{sat} is the value of the polarization on the saturated hysteresis loop at the field of interest, and Γ is a positive function less than or equal to one. Γ is defined as

$$\Gamma = 1 - \tanh\left[\left(\frac{P_d - P_{\text{sat}}}{\xi P_s - P_d}\right)^{\frac{1}{2}}\right] \tag{6}$$

where $\xi = \pm 1$ for increasing or decreasing fields, respectively.

The saturated dipole polarization curve is defined utilizing the hyperbolic tangent function whose behavior satisfies the physical requirements. It is written as a function of the electric field and can be given according to Ref. 31 by

$$P^{+}_{\text{sat}}(E) = P_s \tanh\left[(E - E_c)/2\delta\right] \tag{7}$$

where

$$\delta = E_c \left[\ln\left(\frac{1 + P_r/P_s}{1 - P_r/P_s} \right) \right]^{-1}. \tag{8}$$

By means of an imprint electrical field and its control as per Refs. 20 and 32, we create a memory effect in the initially modeled symmetric butterfly curve. With the imprint electrical field, the D-E hysteresis of the ferroelectric material shifts to the direction of the axis of the electrical field. It can be described as follows,

$$P^{+}_{\text{sat}}(E) = P_s \tanh\left[\frac{(E + \varsigma_s - E_c)[\ln \frac{1+P_r/P_s}{1-P_r/P_s}]}{2E_c} \right] \tag{9}$$

where ς_s presents a shifting factor for the saturation curve.

By eliminating the physical assumption that the two branches of the saturated switching dipole polarization curve are symmetric $P^{-}_{\text{sat}}(E) = -P^{+}_{\text{sat}}(-E)$, we introduce a modification in the original mathematical form where

$$\tanh E = \frac{\sinh E}{\cosh E} \tag{10}$$

by relocating the applied electrical field due to

$$\frac{\sinh(\kappa_s + E)}{\cosh(\kappa_c + E)} \tag{11}$$

where κ_s and κ_c are case-based constants greater or equal to zero with asymmetric relation on the left-hand side or right-hand side, respectively.

C. Sensitivity analysis of the facesheet

A sensitivity analysis is used to obtain the rate of performance measure change with respect to design variable changes. It provides critical information, the gradient, in order to facilitate structural modifications and optimization. Since a thin and compliant facesheet with high reflection is crucial for providing a desired mechanical coupling between actuators and the optical capabilities for the DM, we establish a sensitivity analysis for studying the effect of layer thickness starting from its initial size. This analysis can be extended in case of design changes of the HDM, e.g. structuring the isolation layer in several thin layers of nanometer scale, because it enables a direct comparison between the quantities since the analysis is parametrized based on the mass difference.

When considering the HDM as a framework consisting of thin layers, we want to identify the effects of changing the thicknesses of the individual top layers. Hence, we define the most relevant parameter here to be the thickness of the facesheet t_f. The variable Δm_f defines the mass changes for the facesheet and its relation between added mass Δm, and thickness change Δt, can be given by

$$\Delta m = \rho A \Delta t \tag{12}$$

where ρ presents the density of the material and A the affected area by the thickness change.

The design optimization problem can be posed mathematically by minimizing the objective function which is chosen to be the stiffness ratio S_R. The output of the sensitivity analysis using that function and the differential mass Δm_f is

$$\Theta_f = \frac{\partial S_R}{\partial m_f}. \tag{13}$$

With the assumption that the changes from the current configuration are incrementally small, we expect the change in stiffness ratio to be

$$\Delta S_R = \Theta_f \Delta m_f. \tag{14}$$

III. IMPLEMENTATION AND RESULTS

Section III presents the results of simulations which were made to validate the proposed theoretical frameworks for modeling the HDM as an integrated system including its memory material and a parameter identification for the facesheet. Finite element analyses were performed in Comsol Multiphysics 5.5 and ran in a compute cluster (Peregrine HPC cluster). For all simulations, we used a partition of four Intel Xeon E7 4860v2 or 48 cores @ 2.6 GHz CPUs with 1024 GB or 2048 GB, respectively. Mesh refinement studies were undertaken to ensure convergence of the results.

A. Hysteretic deformable mirror model in 3D

A 3D model of a piezoelectric pellet with thickness t_p and radius r_p was generated in Comsol Multiphysics 5.5 by means of the Structural Mechanics module of Solid Mechanics. The facesheet and isolation layer radii are $r_f = r_s$. The dimensions correspond to the predictions from Ref. 9 and, based on previous studies[4,33–35], adequately dimensioned values based on the forces occurring in the pellet were chosen for the isolation layer and the facesheet. The proposed materials are silicon dioxide and CVD diamond, respectively. Table I summarizes the geometrical parameters used for generating the 3D models.

The bottom of the pellet was mechanically clamped by using the fixed boundary condition. The electrodes were modelled as 2D structures by means of the thin layer boundary condition and were electrically potentialized or grounded, respectively. The surrounding electrodes were provided with a floating potential node. The central actuator of a 5×5 actuator array was addressed as an example in all simulations.

TABLE I: Geometrical parameters for 3D mirror model.

Parameter	Unit	Value
t_p	[mm]	0.25
r_p	[mm]	5
r_f	[mm]	4
r_s	[mm]	4
t_s	[μm]	85
t_f	[nm]	50
Actuator area	[mm^2]	0.25
Actuator spacing	[mm]	0.5

Between the piezoelectric pellet, the isolation layer and facesheet, there is a mechanical contact modelled by introducing contact pairs. Each transition assumes a layer of adhesion which is permanently active so that the upper thin layers are free to move and do not need to be clamped.

The piezoelectric material is based on PZT-5H, contains the modifications from the presented characteristics from Section II B and is implemented as described in Section III B.

B. Memory material implementation

The implementation of the memory material model presented in Section II follows the approach of Ref. 36. The Piezoelectric Devices interface combines Solid Mechanics and Electrostatics together with the constitutive relationships required to model piezoelectrics. Here, the particular material characteristics can be defined by introducing an electric field as a parameter of remanent displacement. In addition, the theoretical relationship between the piezoelectric coefficient d_{mij} is expressed as a derivative of strain to the electric field

$$\begin{aligned} d_{mij} &= \frac{\partial S_{ij}}{\partial E_m} = \frac{Q_{ijkl}P_k\partial P}{\partial E_m} + \frac{Q_{ijkl}P_l\partial P_k}{\partial E_m} \\ &= Q_{ijkl}P_k\varepsilon_{lm} + Q_{ijkl}P_l\varepsilon_{km} \end{aligned} \tag{15}$$

where Q_{ijkl} is the electrostrictive coefficient, ε is the dielectric permittivity, and i, j, k, l and m take the values of 1, 2 or 3.

More specifically, the relationship between the piezoelectric constant d_{33} and electric displacement D for positive and negative applied voltages is introduced in the piezoelectric matrix by

$$d_{33}^{+/-} = 2Q_{33}\varepsilon_{33}^{T}D^{+/-} \tag{16}$$

and

$$d_{33}^{+/-} = d_{32}^{+/-} = 2Q_{12}\varepsilon_{33}^{T}D^{+/-}. \tag{17}$$

In an initial simulation, a sinusoidal voltage is applied to a piezoelectric PNZT ceramic pellet with memory effect (Figure 3) which was modelled in a 2D axisymmetric manner, and a time-dependent study was executed. Using Comsol's finite element nonlinear analysis, the polarization curve and butterfly loop were obtained for the center point of the pellet and presented in Figure 4 and 5. Table II lists the parameters used

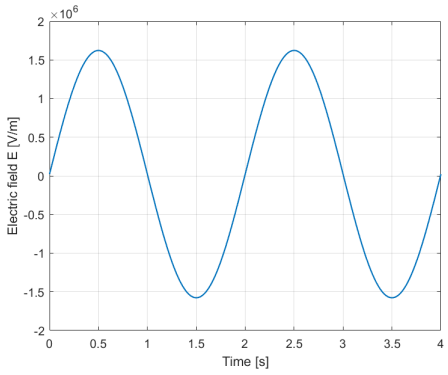

FIG. 3: Sinusoidal voltage applied to the pellet of the modelled PNZT ceramic.

for the implementation of the memory material model (according to the curves exemplified in Figure 2) and the time-dependent simulations. For the remaining materials such as silicon dioxide, CVD diamond and PZT-5H, the material parameters were taken from the Comsol material library.

The results agree with the experimental data from Ref. 9 with exclusive consideration of the memory effect and the significant point of $E = 0$ in the S-E curve of Figure 2 which amounts to approximately 40% of remnant deformation. The slightly lower maximum deformation results from having simulated a thinner pellet.

TABLE II: Parameters for memory material and time-dependent simulations.

Parameter	Unit	Value
Frequency	[Hz]	0.5
P_s	[μC/cm^2]	14.9
P_r	[μC/cm^2]	0.99·P_s
$E_c(+)$	[kV/cm]	12
$E_c(-)$	[kV/cm]	-10
ς_s	[kV/cm]	-7.5
κ_s	[kV/cm]	0
κ_c	[kV/cm]	1

The results of the complex HDM model in 3D were obtained by performing a stationary analysis which initializes the facesheet to a flat surface and, subsequently, another stationary study using these positions as initial input for the remnant deformation by applying $E = 0$ to set the central actuator directly to its memory location. The memory position was energised by using the first point of the asymmetric butterfly loop since the model starts at positive memory position.

Figure 6 shows the contact pressures distribution between the piezoelectric base structure and the top layers. The maximum contact pressure in the memory position amounts to 34.5 MPa while the maximum contact pressure at the maximum deformation of the butterfly loop amounts to approximately 150 MPa. From this, an estimation on the occurring forces for the sensitivity analysis can be made. Figure 7 presents the deformation profile after actuation at $E = 0$ when

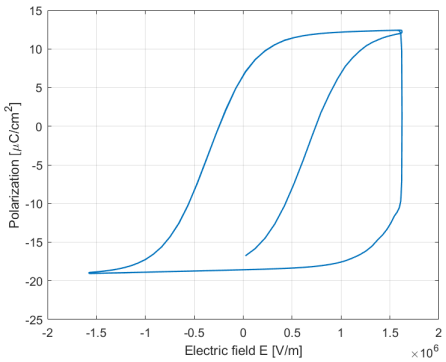

FIG. 4: Polarization hysteresis loop of the modelled HDM memory material. The curve traces the data of the center point of the pellet without upper thin layers of the mirror.

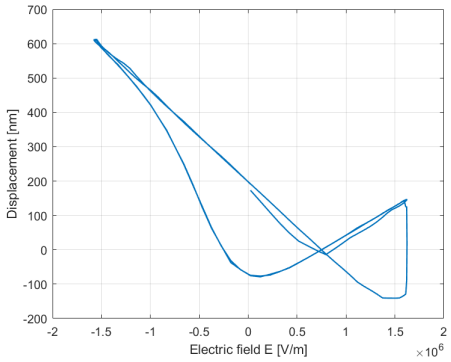

FIG. 5: Strain - Electric field butterfly hysteresis loop with asymmetric shape and memory effect. The curve traces the data of the center point without upper thin layers of the mirror.

making use of the remnant deformation. In this profile, the electrical coupling is already visible due to the distribution of the electric field during actuation. This phenomenon is discussed further in Section III D.

C. Sensitivity of the facesheet

The sensitivity analysis was implemented in a stationary analysis using a PZT-5H base structure of the mirror without the floating potential condition; this was done to consider purely the maximum deformation of the central actuator when addressed with an electrical potential of 650 V at the top electrode while the bottom electrode was grounded. The simulation was solved by using Comsol's forward method due to few scalar parameters to get the sensitivity of the entire solution with respect to the sensitivity variables in addition to the sensitivity of the objective function. The analysis showed that the maximum sensitivity of the facesheet corresponds to $\Theta_f = 7.48$ when the thicknesses of the isolation layer and the facesheet are 85 μm and 50 nm, respectively. Figure 8 shows

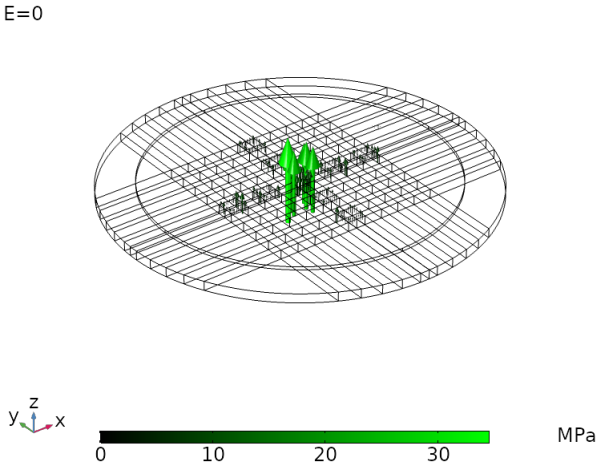

FIG. 6: Contact pressure distribution after actuation of the central actuator when the positions are on hold due to the memory effect. The maximum contact pressure in that position is 34.5 MPa.

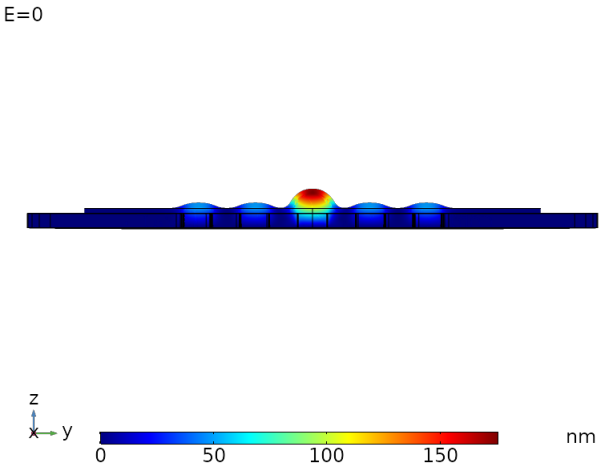

FIG. 7: Cross-section of the deformation profile after actuation of central actuator when the positions are hold due to the memory effect. The maximum deformation in that position amounts to 175 nm. The deformations visualized in the plot are scaled with a factor of 2000 compared to the physical dimensions of the HDM.

the sensitivity of the facesheet. These deformations give a linear approximation of the deformation that would result from a 10 nm increase in the layer thickness. These interactions are the result of bending since the layer becomes stiffer when increasing its thickness.

D. Discussion

Figure 9 shows the HDM in isometric view when there is no voltage applied and the mirror dwells in the memory effect. It is clearly visible that the cross-over actuators are electrically

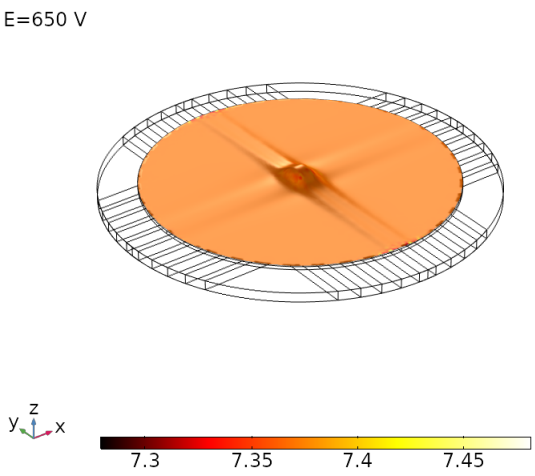

FIG. 8: Sensitivity for the facesheet with a thickness of 50 nm. The deformations give a linear approximation of the deformation that would result from a 10 nm increase of the thickness.

coupled, while the intermediate neighbors are slightly activated. The cross-coupling pervades the mirror surface. This shows the fundamental electrical coupling between the actuators and their position.

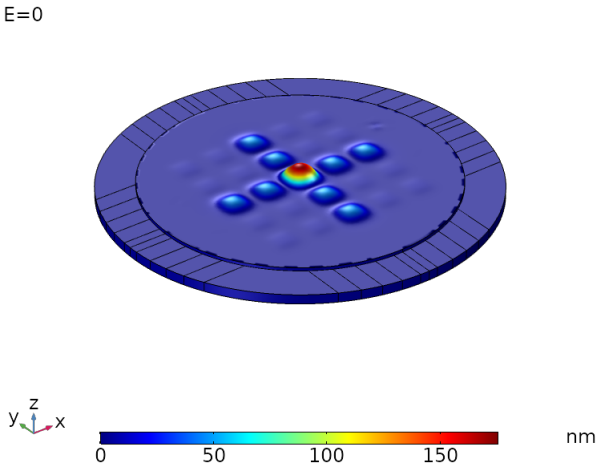

FIG. 9: Isometric view of the HDM when $E = 0$ showing the electrical coupling between the actuators. The maximum deformation of the central actuator amounts to 175 nm, the electrically coupled neighbors on the cross-line have a deformation of approximately 45 nm and the intermediate actuators have a small displacement of < 3 nm. The deformations visualized in the plot are scaled with a factor of 2000 compared to the physical dimensions of the HDM.

Based on the proposed criteria in Section II A, we consider the results and can infer that a primary influence on the cross-over neighbors is present: when the activation threshold of these actuators is reached, they exert a deformation of approximately 48 nm under the given conditions. The intermediate actuators show small deformations ranging from 3 to 5 nm and thus, underlie a secondary influence. These small deformations could be corrected by optimizing geometrical and material parameters and considering the proposed sensitivity analysis in case that the desired accuracy of the mirror is affected. Considering the results of the sensitivity analysis presented in Figure 8, we can see that this adjustment is feasible since the facesheet is already highly sensitive to changes in the order of 10 nm.

IV. CONCLUSION

In this work we studied the influence of the electrical coupling between actuators of the HDM which arises from the proposed electrode layout of the concept and its signal transfer method of TDM. By means of modeling the individual components of the general structure and the memory material of the mirror, we were able to integrate the system in its full complexity in a numerical simulation and draw the conclusion that the major influence is primary for cross-over actuators. In addition, the influence of intermediate actuators is essentially negligible and can be corrected by optimizing the layer thickness with the proposed sensitivity analysis. This summarizes the fundamental electrical coupling relation between the actuators and their position when the central actuator is addressed.

A complex framework was generated which can be used to run virtual experiments with the mirror and help optimizing the design concept of the HDM. Since we experience a more complicated cross-coupling between all actuators of the array in initial 3D time-dependent simulations with an applied electric field in waveform functions for addressing one actuator, further research work is necessary to identify the electric field distribution in possible operating conditions of the HDM. We suggest to disable certain features (dependent on the made assumptions) for reducing the computational effort and simulation time during further simulations to study some aspects in more detail. Hence, simulations such as the optimization of the top layer thicknesses, combinations of addressing certain actuators in time or controlling the electrical coupling by means of different surface initialization become realistic and could be studied.

ACKNOWLEDGMENTS

The authors would like to thank Dr. M. Acuautla and Prof. B. Noheda of the University of Groningen, and Dr. R. Huisman, Dr. S.N.R. Kazmi, M. Eggens and H. Smit of the Netherlands Institute for Space Research for their valuable input on the Hysteretic Deformable Mirror project. In addition, we would like to thank the Center for Information Technology of the University of Groningen for their support and for providing access to the Peregrine high performance computing cluster.

CONFLICTS OF INTEREST

The authors have no conflicts to disclose.

DATA AVAILABILITY STATEMENT

The data that support the findings of this study are available within the article. The complex frameworks and simulation files designed in Comsol Multiphysics of this study are available from the corresponding author upon reasonable request.

[1] K. M. Morzinski, J. W. Evans, S. Severson, B. Macintosh, D. Dillon, D. Gavel, C. Max, and D. Palmer, "Characterizing the potential of MEMS deformable mirrors for astronomical adaptive optics," in *Advances in Adaptive Optics II*, Vol. 6272, edited by B. L. Ellerbroek and D. B. Calia, International Society for Optics and Photonics (SPIE, 2006) pp. 664 – 675.

[2] R. E. Morgan, E. S. Douglas, G. W. Allan, P. Bierden, S. Chakrabarti, T. Cook, M. Egan, G. Furesz, J. N. Gubner, T. D. Groff, C. A. Haughwout, B. G. Holden, C. B. Mendillo, M. Ouellet, P. do Vale Pereira, A. J. Stein, S. Thibault, X. Wu, Y. Xin, K. L. Cahoy, "MEMS Deformable Mirrors for Space-Based High-Contrast Imaging," Micromachines 10 (6), 366 (2019).

[3] V. Mathur, S. R. Vangala, X. Qian, W. D. Goodhue, B. Haji-Saeed, and J. Khoury, "An all optically driven integrated deformable mirror device," Applied Physics Letters 96, 211103 (2010).

[4] Riaud, P., "New high-density deformable mirrors for high-contrast imaging," A&A 545, A25 (2012).

[5] S. Trolier-Mckinstry and P. Muralt, "Thin Film Piezoelectrics for MEMS," Journal of Electroceramics 12, 7–17 (2004).

[6] P. Muralt, R. G. Polcawich, and S. Trolier-McKinstry, "Piezoelectric thin films for sensors, actuators, and energy harvesting," MRS Bulletin 34, 658–664 (2009).

[7] J. Walker, T. Liu, M. Tendulkar, D. N. Burrows, C. T. DeRoo, R. Allured, E. N. Hertz, V. Cotroneo, P. B. Reid, E. D. Schwartz, T. N. Jackson, and S. Trolier-McKinstry, "Design and fabrication of prototype piezoelectric adjustable x-ray mirrors," Opt. Express 26, 27757–27772 (2018).

[8] N. Bishop, J. Walker, C. T. DeRoo, T. Liu, M. Tendulkar, V. Cotroneo, E. N. Hertz, V. Kradinov, E. D. Schwartz, P. B. Reid, T. N. Jackson, and S. Trolier-McKinstry, "Thickness distribution of sputtered films on curved substrates for adjustable x-ray optics," Journal of Astronomical Telescopes, Instruments, and Systems 5, 1 – 14 (2019).

[9] R. Huisman, M. P. Bruijn, S. Damerio, M. J. Eggens, S. N. R. Kazmi, A. E. M. Schmerbauch, H. P. Smit, M. A. Vasquez-Beltran, E. V. der Veer, M. Acuautla, B. Jayawardhana, and B. Noheda, "High pixel number deformable mirror concept utilizing piezoelectric hysteresis for stable shape configurations," Journal of Astronomical Telescopes, Instruments, and Systems 7, 1 – 18 (2021).

[10] R. Hudgin and S. G. Lipson, "Analysis of a monolithic piezoelectric mirror," Journal of Applied Physics 46, 510–512 (1975).

[11] S. Damerio, *Synthesis and implementation of piezoelectric materials as actuators for hysteretic deformable mirrors* (Master Thesis, University of Groningen, 2017).

[12] E. Wainer, "High Titania Dielectrics," Trans. Electrochem. Soc. 89, 47–71 (1946).

[13] A. von Hippel, R. G. Breckenridge, F. G. Chesley, and L. Tisza, "High dielectric constant ceramics," Industrial & Engineering Chemistry 38, 1097–1109 (1946).

[14] S. Roberts, "Dielectric and piezoelectric properties of barium titanate," Phys. Rev. 71, 890–895 (1947).

[15] B. M. Wul and I. M. Goldman, "Dielectric constants of titanates of metals of the second group," Dokl. Akad. Nauk SSSR 46, 154–57 (1945), *Compt. Rend. Acad. Sci. URSS*, 49, 139–42 (1945).

[16] H. Jaffe, "Piezoelectric ceramics," Journal of the American Ceramic Society 41, 494–498 (1958).

[17] B. Jaffe, W. R. Cook Jr., and H. Jaffe, *Piezoelectric Ceramics* (Academic Press, New York, 1971).

[18] G. H. Haertling, "Ferroelectric ceramics: History and technology," Journal of the American Ceramic Society 82, 797–818 (1999).

[19] N. Izyumskaya, Y.-I. Alivov, S.-J. Cho, H. Morkoç, H. Lee, and Y.-S. Kang, "Processing, Structure, Properties, and Applications of PZT Thin Films," Critical Reviews in Solid State and Materials Sciences 32, 111–202 (2007).

[20] T. Morita, Y. Kadota, and H. Hosaka, "Shape memory piezoelectric actuator," Applied Physics Letters 90, 082909 (2007).

[21] R. D. Klissurska, A. K. Tagantsev, K. G. Brooks, and N. Setter, "Use of ferroelectric hysteresis parameters for evaluation of niobium effects in lead zirconate titanate thin films," Journal of the American Ceramic Society 80, 336–342 (1997).

[22] Schmerbauch, A.E.M. and Vakis, A.I. and Huisman, R. and Jayawardhana, B., "Modeling and analysis of a hysteretic deformable mirror with electrically coupled actuators," in *2020 IEEE/ASME International Conference on Advanced Intelligent Mechatronics (AIM)* (2020) pp. 1929–1934.

[23] J. Reiser and H. Marth, "PIRest Technology - How to Keep the Last Position of PZT Actuators without Electrical Power," in *ACTUATOR 2018; 16th International Conference on New Actuators* (2018) pp. 1–4.

[24] L. Dupré, M. De Wulf, D. Makaveev, V. Permiakov, and J. Melkebeek, "Preisach modeling of magnetization and magnetostriction processes in laminated SiFe alloys," Journal of Applied Physics 93, 6629–6631 (2003).

[25] M. Brokate and J. Sprekels, *Hysteresis and Phase Transitions* (New York: Springer-Verlag, 1996).

[26] J.W. Macki, P. Nistri, and P. Zecca, "Mathematical models for hysteresis," SIAM Review 35, 94–123 (1993).

[27] I. Mayergoyz and G. Friedman, "Generalized preisach model of hysteresis," IEEE Transactions on Magnetics 24, 212–217 (1988).

[28] G.-Y. Gu, L.-M. Zhu, C.-Y. Su, H. Ding, and S. Fatikow, "Modeling and control of piezo-actuated nanopositioning stages: A survey," IEEE Transactions on Automation Science and Engineering 13, 313–332 (2016).

[29] K. Lim, K. Kim, S. Hong, and K. Lee, "A semi-empirical cad model of ferroelectric capacitor for circuit simulation," Integrated Ferroelectrics 17, 97–104 (1997).

[30] S. L. Miller, R. D. Nasby, J. R. Schwank, M. S. Rodgers, and P. V. Dressendorfer, "Device modeling of ferroelectric capacitors," Journal of Applied Physics 68, 6463–6471 (1990).

[31] S. L. Miller, J. R. Schwank, R. D. Nasby, and M. S. Rodgers, "Modeling ferroelectric capacitor switching with asymmetric nonperiodic input signals and arbitrary initial conditions," Journal of Applied Physics 70, 2849–2860 (1991).

[32] Y. Kadota, H. Hosaka, and T. Morita, "Shape memory piezoelectric actuator by control of the imprint electrical field," Ferroelectrics 368, 185–193 (2008).

[33] R. Hamelinck, N. Rosielle, P. Kappelhof, B. Snijders, and M. Steinbuch, "A large adaptive deformable membrane mirror with high actuator density," in *Advancements in Adaptive Optics*, Vol. 5490, edited by D. B. Calia, B. L. Ellerbroek, and R. Ragazzoni, International Society for Optics and Photonics (SPIE, 2004) pp. 1482 – 1492.

[34] T. G. Bifano, J. A. Perreault, P. A. Bierden, and C. E. Dimas, "Micromachined deformable mirrors for adaptive optics," in *High-Resolution Wavefront Control: Methods, Devices, and Applications IV*, Vol. 4825, edited by J. D. Gonglewski, M. A. Vorontsov, M. T. Gruneisen, S. R. Restaino, and R. K. Tyson, International Society for Optics and Photonics (SPIE, 2002) pp. 10 – 13.

[35] M. Sato, I. Kanno, H. Kotera, and O. Tabata, "Piezoelectric mems deformable mirrors with high-density actuator array," in *2011 IEEE 24th International Conference on Micro Electro Mechanical Systems* (2011) pp. 1265–1268.

[36] A. López, A. De Andrés, and P. Ramos, "Finite element model of a ferroelectric," in *COMSOL Conference Proceeding, Paris 2010* (2011).